Correspondence

A Computationally Efficient Technique for Estimating the Parameters of Polynomial-Phase Signals From Noisy Observations

Maree Farquharson, Peter O'Shea, and Gerard Ledwich

***Abstract*—Many real-world applications are characterized by the presence of polynomial phase signals embedded in noise. These applications include radar, sonar, telemetry, communications, and power systems. In a significant number of these applications, it is highly desirable to be able to accurately estimate the polynomial phase signal parameters. This correspondence presents a computationally efficient method for estimating any or all of the parameters of polynomial-phase signals in white Gaussian noise and provides a first-order statistical analysis of the technique. Simulations are also presented to support the theoretical analysis.**

***Index Terms*—Higher order statistics, parameter estimation, polynomial approximation.**

I. Introduction

Let $z_s(n)$ be a noiseless discrete-time polynomial phase signal (PPS) defined as

$$z_s(n) = b_0 e^{j\phi(n)}, \quad -\frac{N-1}{2} \le n \le \frac{N-1}{2} \tag{1}$$

where

$$\phi(n) = \sum_{p=0}^{P} a_p n^p. \tag{2}$$

In (1) and (2), P is the order of the polynomial phase, the $\{b_0, a_0, a_1, a_2, \ldots, a_P\}$ are unknown parameters, N is an odd integer, and the sampling rate is unity. In order to avoid ambiguities arising from the cyclic nature of spectral transforms of sampled signals [1], it is assumed that

$$|a_p| \le \frac{\pi}{p!\left(\frac{N}{2}\right)^{(p-1)}}, \quad p = 1, 2, \ldots, P. \tag{3}$$

A noisy signal $z_r(n)$ is formed by adding complex, white, Gaussian noise $z_w(n)$ to $z_s(n)$:

$$z_r(n) = z_s(n) + z_w(n). \tag{4}$$

The complex noise $z_w(n)$ has a variance of σ^2. Estimation of the unknown parameters from $z_r(n)$ is an important problem. The obvious solution is the direct maximum likelihood (ML) method, but this approach requires a P-dimensional search and, therefore, is very computationally intensive. The ML method also requires very good initial estimates to initiate a gradient search, necessitating very fine searches. To offset problems with computational burden, various authors have developed alternative strategies [1]–[5]. Most of these are based on multilinear transforms that require P one-dimensional searches rather than one P-dimensional search. Recently, a bilinear transform known as the cubic phase (CP) function was introduced and shown to be very effective for parameter estimation of third-order PPSs [6]. Multilinear extensions of this function, which were referred to as the "higher order phase (HP) functions," were also introduced briefly in [7], specifically for the purposes of parameter estimation of polynomial-phase signals of order greater than 3. This paper presents a broadening of the class of discrete-time HP functions presented in [7], with this broadened class allowing more flexibility in the estimation of polynomial phase parameters. This new class of functions has a lot of similarities to the "discrete generalized Wigner distributions" documented in [4] but also has some significant differences. The formulation proposed in this correspondence gives rise to parameter estimates whose asymptotic mean-square errors (AMSEs) are typically lower than those derived from the algorithm in [4].

The new class of discrete-time HP functions is defined in Section II. An algorithm for estimating the polynomial phase parameters is presented in Section III. Section IV provides simulation results obtained after applying the algorithm to a synthetic PPS, whereas Section V is devoted to a discussion. Section VI presents the conclusions. Derivations of AMSEs for the parameter estimates are done in the Appendix.

II. Higher Order Phase Functions

The purpose of the HP functions is to transform a signal into a domain that enhances the parameter of interest. This transformation involves a two-step procedure. Step a) performs a multilinear operation on the signal to obtain a suitable "kernel," and step b) applies a phase matching operator to this kernel to yield an energy concentration around the parameter of interest. The kernel mentioned above is as in (5), shown at the bottom of the next page, where $K_{z_r}^p(n,m)$ is the kernel of $z_r(n)$ for the pth-order HP function, and I is the "order" of the kernel. The lag coefficients c_i are real (i.e., $\{c_i\}_{i=1}^{I/2} \in \Re$), and the maximum lag value is given by $c_{\max} = \max\{abs(c_i)\}_{i=1}^{I/2}$. The notation $\{\cdot\}^{*u_i}$ signifies that $\{\cdot\}$ is conjugated if u_i is 1 and that $\{\cdot\}$ is not conjugated if u_i is 0. The $\{c_i\}$ are assumed to be distinct, and the values for $\{I, \{c_i\}, \{u_i\}, i = 1, \ldots, I/2\}$ are selected to ensure that for a PPS signal, $K_{z_r}^p(n,m)|_{n=0}$ evaluates to a constant amplitude term with only pth- and 0th-order phase components:

$$\begin{aligned} K_{z_s}^p(n,m)|_{n=0} &= K_{z_s}^p(m) \\ &= b_0^I \cdot \exp\left(\frac{j a_p p! m^p}{c_{\max}^p} + j\varsigma\right) \end{aligned} \tag{6}$$

where $\varsigma = (I - 4\sum_{i=1}^{I/2} u_i)a_0$ if p is even and $\varsigma = 0$ if p is odd. That is, following a similar approach to that used in [3] for designing the polynomial Wigner–Ville distributions (PWVDs), the $\{I, \{c_i\}, \{u_i\}, i = 1, \ldots, I/2\}$ values are chosen so that at time $n = 0$, the kernel contains only a pth-order phase term and (possibly) a 0th-order phase term. Furthermore, the coefficient for the pth-order phase term on the right-hand side of (6) is chosen to be the (scaled) instantaneous $(p-1)$th-order frequency derivative of the signal at $n = 0$. To achieve this form for the kernel, one can use (1), (5), and (6) to set up (and solve) a set of nonlinear equations. A key issue in setting up these equations is selection of the value of I. First, I must be even so that $I/2$ in (5) is an integer. Second, I must be chosen such that the construction of the set

Manuscript received December 10, 2003; revised October 7, 2004. This work was supported by a Queensland University of Technology Small Research Grant. The associate editor coordinating the review of this manuscript and approving it for publication was Prof. Fredrik Gustafsson.

The authors are with the School of Electrical and Electronic Systems Engineering, Queensland University of Technology, Brisbane, 4001, Australia (e-mail: ml.farquharson@student.qut.edu.au; pj.oshea@qut.edu.au; g.ledwich@qut.edu.au).

Digital Object Identifier 10.1109/TSP.2005.851177

of nonlinear equations yields at least as many c_i values as there are equations. This implies that when P (the polynomial order) is even, $I \geq P$, and when P is odd, $I \geq \begin{cases} (P-1), & \text{for } \hat{a}_2, \hat{a}_4, \ldots \\ (P+1), & \text{for } \hat{a}_3, \hat{a}_5, \ldots \end{cases}$. A further constraint on I arises from the fact that the c_i values should be real and distinct. The recommended procedure for selecting I is thus to initially set $I = P$ if P is even and set $I = \begin{cases} (P-1), & \text{for } \hat{a}_2, \hat{a}_4, \ldots \\ (P+1), & \text{for } \hat{a}_3, \hat{a}_5, \ldots \end{cases}$ if P is odd. If the set of c_i values found using this value of I is real and distinct, then terminate; otherwise, iteratively increase I by 2 until one can find c_i values that are real and distinct.

When I is found, a range of possible solutions will typically exist for the $\{c_i\}$. There are a number of ways to select the "best" solution from this range of possible solutions. One way is to choose the solution that gives rise to the minimum AMSE for the relevant parameter estimate at high signal-to-noise ratio (SNR). (Note that formulae for the AMSEs in terms of the $\{c_i\}$ are contained in the Appendix). Using this approach for P = 4, for example, gives rise to the coefficients in the following.

$$\begin{aligned}
&\text{For estimating } \hat{a}_1: \mathrm{c}_1 = 0.721\,99, c_2 = 0.638\,01 \\
&\qquad\qquad c_3 = -0.86. \\
&\text{For estimating } \hat{a}_2: \mathrm{c}_1 = 1.5547, c_2 = 1.323\,97, c_3 = 1.29 \\
&\qquad\qquad u_1 = 1, u_2 = 0, u_3 = 0. \\
&\text{For estimating } \hat{a}_3: \mathrm{c}_1 = 1.6056, c_2 = -0.6556 \\
&\qquad\qquad c_3 = -0.95. \\
&\text{For estimating } \hat{a}_4: \mathrm{c}_1 = 2.2134, c_2 = 1.5602 \\
&\qquad\qquad c_3 = 1.57, u_1 = 0, u_2 = 1, u_3 = 1.
\end{aligned}$$

Then, the kernel needed to estimate $\hat{a}_4$, for example, from a fourth-order PPS would be [using the above coefficients and (6)]

$$\begin{aligned}
K^4_{z_s}(n,m)|_{n=0} &= K^4_{z_s}(m) \\
&= b_0^6 \cdot \exp\left(\frac{j24a_4m^4}{(2.2134)^4} + j2a_0\right). \qquad (7)
\end{aligned}$$

Note that computation of the samples in the kernel requires the availability of samples of $z_r(n)$ at noninteger values of n. A lowpass interpolation filter (using, for example, MATLAB's "interp" command) can be used to obtain the required noninteger samples. It is assumed in this paper that ideal ("sinc function") interpolation is used, and a statistical analysis done within the Appendix is performed under that assumption. In practice, however, it has been found that if MATLAB's "interp" command is used with an interpolation factor of 8, performance is very similar to using ideal interpolation. Once the kernel has been computed, it is necessary to try and create an energy concentration around the a_p parameter value. This can be done by applying a classical phase-matching transform to the kernel. The HP functions are constituted by the phase matching transforms applied to the kernel and are defined as (8), shown at the bottom of the page. Note that the $\mathrm{HP}^p_{z_r}(n,\Omega_p)$ function has an interpretation as a "time—$(p-1)$th-order frequency derivative" representation. That is, the $\mathrm{HP}^p_{z_r}(n,\Omega_p)$ function exhibits an energy concentration around the (scaled) $(p-1)$th-order derivative of the signal's instantaneous frequency law. Note also that $\mathrm{HP}^1_{z_r}(n,\Omega_1)$ is essentially the PWVD function defined in [3] and is a time-frequency representation. That is, $\mathrm{HP}^1_{z_r}(n,\Omega_1)$ exhibits an energy concentration around the instantaneous frequency law of the signal.

Any or all of the $\{\hat{a}_p, p = 1,2,\ldots,P\}$ can be obtained by evaluating the appropriate HP function at $n = 0$ and finding where the maximum occurs. This estimation process is specified by

$$\begin{aligned}
\hat{a}_p &= \arg\max_{\Omega_p} \left\{\left|\mathrm{HP}^p_{z_r}(n=0,\Omega_p)\right|\right\} \\
&= \arg\max_{\Omega_p} \left\{\left|\mathrm{HP}^p_{z_r}(\Omega_p)\right|\right\}, \quad p = 1,2,\ldots,P. \qquad (9)
\end{aligned}$$

Note that if one sets $p = 2$ in (8), one obtains, up to a frequency-rate scaling factor, the more restricted class of HP functions described in [7]. In order to see how the HP functions compare with the discrete generalized Wigner distributions (DGWDs) defined in [4], one has to compare (5) and (8) in this paper with [4, eq. (62)]. The HP functions have a similar form to the DGWDs but also differ in that i) they have a different structure for even and odd values of p, ii) they incorporate a "lag and frequency scaling operation," and iii) they have different kernel orders to those proposed in [4].

III. Outline of the Parameter Estimation Algorithm

If all the phase parameters in the observation need to be estimated, the following algorithm can be used.

a) Calculate all P higher order phase parameter estimates (i.e., find $\hat{a}_p, p = 1,2,\ldots,P$) using (9).

b) Calculate the initial phase parameter estimate by appropriately scaling the phase at the peak value of the second-order HP function:

$$\hat{a}_0 = \frac{1}{\left(I - 4\sum_{i=1}^{I/2} u_i\right)} \times \Im\left\{\log\left(\frac{2}{N}\left(\sum_{m=0}^{\frac{(N-1)}{2}} K^2_{z_r}(0,m) e^{-j\frac{2\hat{a}_2 m^2}{c^2_{\max}}}\right)\right)\right\}. \qquad (10)$$

c) Determine $\hat{b}_0$ as specified in

$$\hat{b}_0 = \frac{|z_{de}|}{N} \quad \text{where } z_{de} = \sum_{n=-\frac{(N-1)}{2}}^{n=\frac{(N-1)}{2}} z_r(n) e^{-j\sum_{p=1}^{P} \hat{a}_p n^p}. \qquad (11)$$

Note that if only some (rather than all) of the phase parameters need to be estimated, then only some of the HP functions need to be computed. If, for example, only one of the a_p parameters needs to be estimated, then only one HP function needs to be

$$K^p_{z_r}(n,m) = \begin{cases} \prod_{i=1}^{I/2} \left[z_r\left(n + \frac{mc_i}{c_{\max}}\right) z_r\left(n - \frac{mc_i}{c_{\max}}\right)\right]^{*u_i}, & \text{for } m = 0,1,\ldots,\frac{N-1}{2} - |n|, \quad p = 2,4,\ldots \\ \prod_{i=1}^{I/2} \left[z_r\left(n + \frac{mc_i}{c_{\max}}\right) z_r^*\left(n - \frac{mc_i}{c_{\max}}\right)\right], & \text{for } |m| = 0,1,\ldots,\frac{N-1}{2} - |n|, \quad p = 1,3,\ldots \end{cases} \qquad (5)$$

$$\mathrm{HP}^p_{z_r}(n,\Omega_p) = \begin{cases} \sum_{m=0}^{\frac{(N-1)}{2}} K^p_{z_r}(n,m) e^{-j\frac{\Omega_p p! m^p}{c^p_{\max}}}, & \text{for } p = 2,4,6,\ldots \\ \sum_{m=-\frac{(N-1)}{2}}^{\frac{(N-1)}{2}} K^p_{z_r}(n,m) e^{-j\frac{\Omega_p p! m^p}{c^p_{\max}}}, & \text{for } p = 1,3,5,\ldots \end{cases} \qquad (8)$$

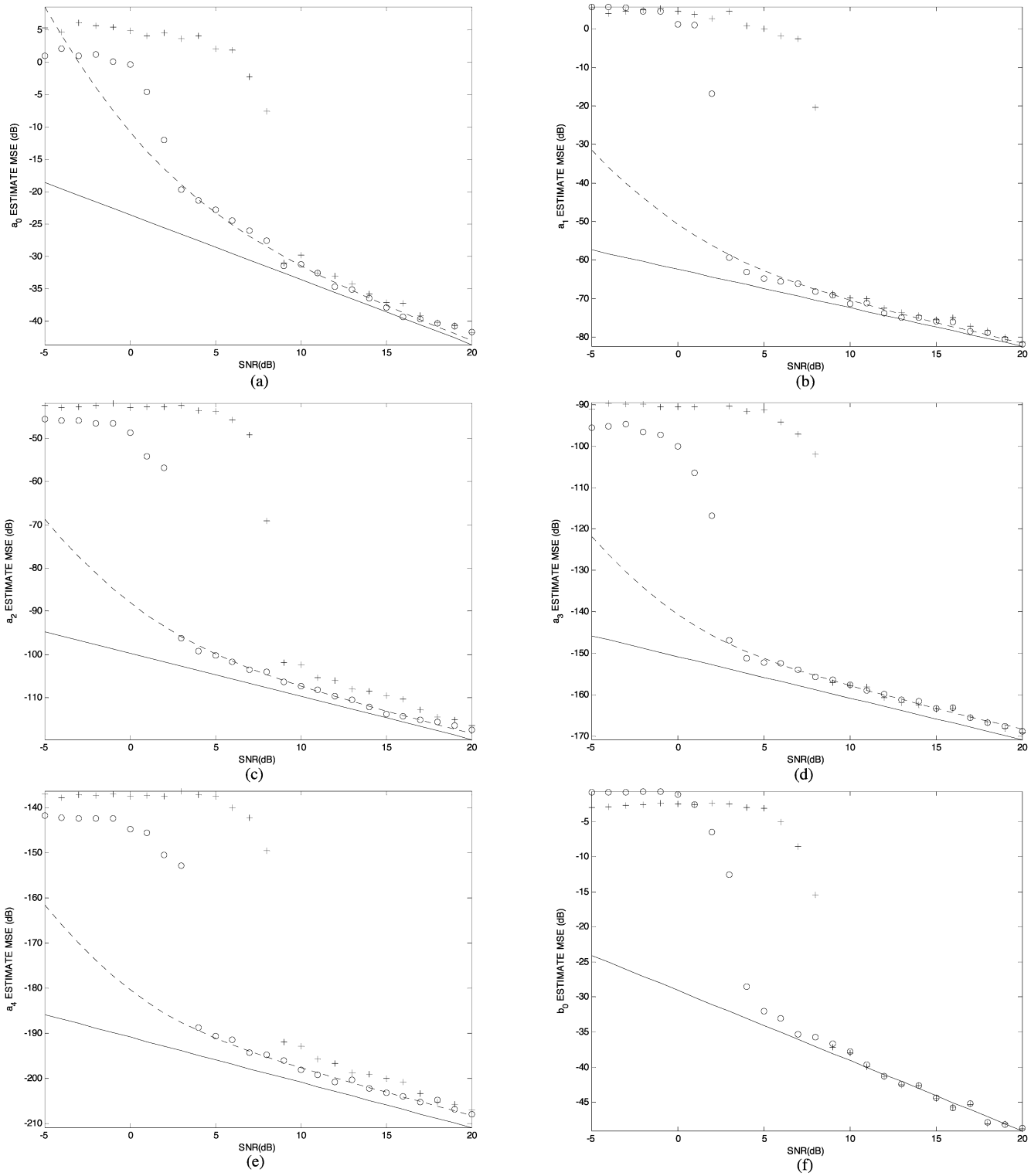

Fig. 1. MSEs versus SNR for all of the parameter estimates. Full line: CR bound. Dashed line: theoretically predicted MSEs. Circles: HP function-based MSEs. Plus signs: HAF-based MSEs. (a) a_0 estimate MSE versus SNR. (b) a_1 estimate MSE versus SNR. (c) a_2 estimate MSE versus SNR. (d) a_3 estimate MSE versus SNR. (e) a_4 estimate MSE versus SNR. (f) b_0 estimate MSE versus SNR.

calculated. This is not the case in general for the rival method in [1]; for that method, it is typically necessary to compute several multilinear functions, even if there is only one parameter to be estimated. Note also that step b) is only one of many ways that a_0 can be estimated. It can be estimated i) by extracting the phase at the peak of $\mathrm{HP}^2_{z_r}(0,\Omega_p)$, as recommended above, ii) by extracting the phase at the peak of any of the other $\mathrm{HP}^p_{z_r}(0,\Omega_p)$ functions for which p is even, or iii) by extracting the phase of z_{de}. Simulations to date have shown that option i) tends to yield the lowest AMSE and is recommended for this reason. Similarly, one can estimate b_0 other than via (11), but no alternative has been found to work better.

IV. Simulations

The estimation algorithm in Section III was applied to a fourth-order polynomial phase signal submerged in additive, complex, white, zero mean Gaussian noise for a range of different noise levels. These noise levels corresponded to the SNR range of -5 to 20 dB. The number of Monte Carlo simulations was 100, and there were 401 samples in the observation. For comparison purposes, the signal's parameter values were chosen to be the same values as in the example in [8, Sec. IV], i.e., $a_0 = 0.2, a_m = 4/(N^m)$, and $b_0 = 1$. Fig. 1(a)–(f) shows the mean-square errors (MSEs) of the HP function-based parameter estimates (denoted with circles) and the High-Order Ambiguity Function [1] (HAF)-based estimates (denoted with plus signs) for different SNRs.

V. Discussion

The figures show that the simulation results for the HP function method are very close to the theoretically predicted results and close to the CR bounds at high SNR. At very high SNRs, $\hat{a}_0, \hat{a}_1, \hat{a}_2, \hat{a}_3$, and $\hat{a}_4$ were found to have MSEs that were, respectively, $\sim 0.51, 0.73, 1.27$, 2.39, and 2.62 dB above the CR bound. The HP function-based MSEs compare well with the HAF-based MSEs for all parameters at all SNRs. The SNR threshold for the HP function-based estimates ranges between 3 and 4 dB (depending on the parameter). This threshold is lower than the thresholds observed in [8] for i) the HAF method (11 dB), ii) the product HAF (PHAF) method (6 dB), and iii) the phase unwrapping and least-squares fitting (PULS) method (9 dB).

The HP function method, because it can be implemented with subband decomposition in the $(p-1)$ *th-order frequency derivative* domain, requires relatively little computation. i.e., it requires only a few times $PN\log(N)$ operations. This amounts to a few times 14 400 operations for the 400-point signal used for the simulations. The HAF method has a similar computational burden to the HP function method, whereas the PHAF requires more computation than the HAF method again because several HAFs must be computed to form each product. The PULS method is particularly efficient, requiring only a few multiples of PN operations, but it is only effective above about 9 dB. It is possible to achieve quite low SNR thresholds by using methods with more computation. The direct ML method, for example, has a significantly lower SNR threshold (about -8 dB) but requires $O(N^P \log N)$ operations. The higher order integrated ambiguity function method is another alternative for PPS analysis. It uses two-dimensional rather than P-dimensional searches. The reduced dimensionality yields computation of $O(N^2 \log N)$, but the statistical performance is significantly poorer than the ML method. Another approach that can be used is the "nonlinear instantaneous least-squares (NILS) approach" [8]. This method uses conditioning strategies to enable relatively efficient, iterative multidimensional gradient-based searches to be implemented. It has not been established with certainty if convergence will occur under all relevant conditions, but the simulations that have been conducted have been successful. If the kind of gradient search routines described in [9] are used for the algorithm in [8], then one requires a few multiples of $KL(2)P^2N$ operations, where L is the number of iterations required for convergence, and K is the number of sliding window length iterations used [8]. For the 400-sample fourth-order PPS signal used in the simulations, if $K = 4$ and $L = 4$, then the computation would be a few multiples of 204 800 operations. This is a modest amount of computation compared with the ML method but is significantly more than for the HP function method for the same signal. The threshold reported in [8] for the NILS method is about -6 dB.

VI. Conclusion

Many real-world applications contain signals that can be modeled as polynomial phase signals. Many of these applications require information about frequency trajectory and, therefore, about the polynomial phase parameters. This correspondence has presented a computationally efficient technique that gives accurate estimates for the polynomial phase parameters at moderate to high SNR. The AMSE derivations for the parameter estimates have produced results that line up very closely with those observed in simulation.

Appendix

This Appendix derives the asymptotic (i.e., large sample) mean-square errors for the unknown parameter estimates. The derivations are complicated somewhat by the fact that the noise in the kernel is *not* white for many useful values of the $\{c_i\}$. This is the case even if the noise on the original observation is white. The derivations in this Appendix follow the approach used in [10]. It is assumed that the parameter values $\{\hat{a}_p, p = 0, 1, \ldots, P\}$ and $\hat{b}_0$ deviate from the true parameter values by $\{\delta a_p, p = 0, 1, \ldots, P\}$ and δb_0, respectively, i.e.,

$$\hat{a}_p = a_p + \delta a_p, \quad \text{for } p = 0, 1, \ldots, P \quad \text{and} \quad \hat{b}_0 = b_0 + \delta b_0. \tag{12}$$

A. Asymptotic Mean Square Error Derivation for $\hat{a}_p, p = 1, 2, \ldots, P$

The $\{\hat{a}_p\}$ are determined according to (9). The SNR is defined as SNR $= (b_0^2/\sigma^2)$. The formulae required for determining the AMSEs for the $\{\hat{a}_p\}$ were obtained from [10, App.] and are given in (13)–(17), shown at the bottom of the page, and $\Re\{\cdot\}$ signifies the real part of $\{\cdot\}$. Note that in the above, B is a random quantity, but A is deterministic because all constituent terms are derived from the noise-free signal. Equations (6), (8), and (14)–(17) were used to determine the

$$E[(\delta a_p)^2] = \frac{E[B^2]}{A^2} \tag{13}$$

$$A = 2\Re\left\{ \mathrm{HP}^p_{z_s}(a_p) \frac{\partial^2 \mathrm{HP}^{p^*}_{z_s}(a_p)}{\partial \Omega_p^2} + \frac{\partial \mathrm{HP}^p_{z_s}(a_p)}{\partial \Omega_p} \frac{\partial \mathrm{HP}^{p^*}_{z_s}(a_p)}{\partial \Omega_p} \right\} \tag{14}$$

$$B = 2\Re\left\{ \mathrm{HP}^p_{z_s}(a_p) \frac{\partial \delta \mathrm{HP}^{p^*}_{z_s}(a_p)}{\partial \Omega_p} + \frac{\partial \mathrm{HP}^p_{z_s}(a_p)}{\partial \Omega_p} \delta \mathrm{HP}^{p^*}_{z_s}(a_p) \right\} \tag{15}$$

$$\delta \mathrm{HP}^p_{z_r}(\Omega_p) = \begin{cases} \sum_{m=0}^{\frac{(N-1)}{2}} z_{ws}(m) e^{-j \frac{\Omega_p p! m^p}{c^p_{\max}}}, & p = 2, 4, \ldots \\ \sum_{m=-\frac{(N-1)}{2}}^{\frac{(N-1)}{2}} z_{ws}(m) e^{-j \frac{\Omega_p p! m^p}{c^p_{\max}}}, & p = 1, 3, \ldots \end{cases} \tag{16}$$

$$z_{ws}(m) = K^p_{z_r}(0, m) - K^p_{z_s}(0, m) \tag{17}$$

results in (18)–(20), shown at the bottom of the page, where $\Im\{\cdot\}$ denotes the imaginary part of $\{\cdot\}$, as well as (21), shown at the bottom of the page. Note that in the above, ideal interpolation (i.e., a sinc function impulse response filter) has been assumed.

B. Mean Square Errors for the a_0 and b_0 Estimates

The b_0 and a_0 estimates are determined in a similar fashion to [10]. The results are

$$E\{(\delta b_0)^2\} \approx \frac{\sigma^2}{2N} \tag{22}$$

$$\begin{aligned}
&E[(\delta a_0)^2] \\
&\quad\approx \frac{1}{\left(I-4\sum_{i=1}^{I/2} u_i\right)^2}\left(\frac{N^4 E[(\delta a_2)^2]}{36c_{\max}^4}-\frac{60}{N^4\mathrm{SNR}}\right.\\
&\qquad\times\sum_{m_1=0}^{\frac{N}{2}}\left[\left(m_1^2-\frac{N^2}{12}\right)\sum_{m_2=0}^{\frac{N}{2}}\left[\sum_{j=1}^{\frac{I}{2}}\sum_{k=1}^{\frac{I}{2}}\left((-1)^{(u_j+u_k)}\right.\right.\right.\\
&\qquad\times\operatorname{sinc}\left(\frac{c_k}{c_{\max}}m_2-\frac{c_j}{c_{\max}}m_1\right)\\
&\qquad+(-1)^{(u_j+u_k)}\operatorname{sinc}\left(\frac{c_k}{c_{\max}}m_2+\frac{c_j}{c_{\max}}m_1\right)\\
&\qquad+(-1)^{(u_j+u_k)}\operatorname{sinc}\left(-\frac{c_k}{c_{\max}}m_2-\frac{c_j}{c_{\max}}m_1\right)\\
&\qquad\left.\left.\left.+(-1)^{(u_j+u_k)}\operatorname{sinc}\left(-\frac{c_k}{c_{\max}}m_2+\frac{c_j}{c_{\max}}m_1\right)\right)\right]\right]\\
&\qquad+\frac{1}{N}\left(\left(1+\frac{1}{\mathrm{SNR}}\right)^I-\frac{(I+\mathrm{SNR})}{\mathrm{SNR}}\right)\\
&\qquad+\frac{b_0^{2I}}{2\mathrm{SNR}}\sum_{m_1=0}^{\frac{N}{2}}\left[\sum_{m_2=0}^{\frac{N}{2}}\left[\sum_{j=1}^{\frac{I}{2}}\sum_{k=1}^{\frac{I}{2}}\left((-1)^{(u_j+u_k)}\right.\right.\right.\\
&\qquad\times\operatorname{sinc}\left(\frac{c_k}{c_{\max}}m_2-\frac{c_j}{c_{\max}}m_1\right)\\
&\qquad+(-1)^{(u_j+u_k)}\operatorname{sinc}\left(\frac{c_k}{c_{\max}}m_2+\frac{c_j}{c_{\max}}m_1\right)\\
&\qquad+(-1)^{(u_j+u_k)}\operatorname{sinc}\left(-\frac{c_k}{c_{\max}}m_2-\frac{c_j}{c_{\max}}m_1\right)\\
&\qquad\left.\left.\left.+(-1)^{(u_j+u_k)}\operatorname{sinc}\left(-\frac{c_k}{c_{\max}}+\frac{c_j}{c_{\max}}m_1\right)\right)\right]\right]
\end{aligned} \tag{23}$$

and $E[(\delta a_2)^2]$ is obtained by substituting $p=2$ into (20).

$$A\approx\begin{cases}-\dfrac{2b_0^{2I}(p!)^2p^2N^{2(p+1)}}{c_{\max}^{2p}2^{2(p+1)}(2p+1)(p+1)^2}, & \text{for } p=2,4,\ldots\\ -\dfrac{4b_0^{2I}(p!)^2N^{2(p+1)}}{c_{\max}^{2p}(2p+1)2^{(2p+1)}}, & \text{for } p=1,3,\ldots\end{cases} \tag{18}$$

$$B\approx\begin{cases}-\dfrac{b_0^INp!}{c_{\max}^p}\Im\left\{e^{ja_0\left(I-4\sum_{i=1}^{I/2}u_i\right)}\sum_{m=0}^{\frac{N}{2}}\left(m^p-\frac{N^p}{2^p(p+1)}\right)z_{ws}^*(m)e^{\frac{ja_pp!m^p}{c_{\max}^p}}\right\}, & \text{for } p=2,4,\ldots\\ -\dfrac{2b_0^INp!}{c_{\max}^p}\Im\left\{\sum_{m=-\frac{N}{2}}^{\frac{N}{2}}m^pz_{ws}^*(m)e^{\frac{ja_pp!m^p}{c_{\max}^p}}\right\}, & \text{for } p=1,3,\ldots\end{cases} \tag{19}$$

$$E[(\delta a_p)^2]\approx\begin{cases}\dfrac{4c_{\max}^{2p}2^{4p}(2p+1)^2(p+1)^4}{b_0^{2I}(p!)^2p^4N^{2(2p+1)}}V_{\ker n}, & \text{for } p=2,4,\ldots\\ \dfrac{c_{\max}^{2p}2^{4p}(2p+1)^2}{b_0^{2I}(p!)^2N^{2(2p+1)}}V_{\ker n}, & \text{for } p=1,3,\ldots\end{cases} \tag{20}$$

$$\begin{aligned}
V_{\ker n}\approx\begin{cases}
&\dfrac{N^{(2p+1)}p^2}{(p+1)^2(2p+1)2^{(2p+1)}}\dfrac{b_0^{2I}}{2}\left(\left(1+\dfrac{1}{\mathrm{SNR}}\right)^I-\dfrac{(I+\mathrm{SNR})}{\mathrm{SNR}}\right)\\
&+\dfrac{b_0^{2I}}{2\mathrm{SNR}}\sum_{m_1=0}^{\frac{N}{2}}\left[\sum_{m_2=0}^{\frac{N}{2}}\left[(m_1^p-N^p/(2^p(p+1)))(m_2^p-N^p/(2^p(p+1)))\right.\right.\\
&\times\sum_{j=1}^{\frac{I}{2}}\sum_{k=1}^{\frac{I}{2}}\left((-1)^{(u_j+u_k)}\operatorname{sinc}\left(\frac{c_k}{c_{\max}}m_2-\frac{c_j}{c_{\max}}m_1\right)+(-1)^{(u_j+u_k)}\operatorname{sinc}\left(\frac{c_k}{c_{\max}}m_2+\frac{c_j}{c_{\max}}m_1\right)\right.\\
&\left.\left.\left.+(-1)^{(u_j+u_k)}\operatorname{sinc}\left(-\frac{c_k}{c_{\max}}m_2-\frac{c_j}{c_{\max}}m_1\right)+(-1)^{(u_j+u_k)}\operatorname{sinc}\left(-\frac{c_k}{c_{\max}}m_2+\frac{c_j}{c_{\max}}m_1\right)\right)\right]\right], & \text{for } p=2,4,\ldots\\
&\dfrac{N^{(2p+1)}b_0^{2I}}{(2p+1)2^{2p}}\left(\left(1+\dfrac{1}{\mathrm{SNR}}\right)^I-\dfrac{(I+\mathrm{SNR})}{\mathrm{SNR}}\right)\\
&+\dfrac{2b_0^{2I}}{\mathrm{SNR}}\sum_{m_1=0}^{\frac{N}{2}}\left[m_1^p\sum_{m_2=0}^{\frac{N}{2}}\left[m_2^p\sum_{j=1}^{\frac{I}{2}}\sum_{k=1}^{\frac{I}{2}}\left(\operatorname{sinc}\left(\frac{c_k}{c_{\max}}m_2-\frac{c_j}{c_{\max}}m_1\right)-\operatorname{sinc}\left(\frac{c_k}{c_{\max}}m_2+\frac{c_j}{c_{\max}}m_1\right)\right.\right.\right.\\
&\left.\left.\left.-\operatorname{sinc}\left(-\frac{c_k}{c_{\max}}m_2-\frac{c_j}{c_{\max}}m_1\right)+\operatorname{sinc}\left(-\frac{c_k}{c_{\max}}m_2+\frac{c_j}{c_{\max}}m_1\right)\right)\right]\right], & \text{for } p=1,3,\ldots
\end{cases}
\end{aligned} \tag{21}$$

REFERENCES

[1] S. Peleg and B. Friedlander, "The discrete polynomial-phase transform," *IEEE Trans. Signal Process.*, vol. 43, no. 8, pp. 1901–1914, Aug. 1995.

[2] S. Barbarossa, A. Scaglione, and G. B. Giannakis, "Product high-order ambiguity function for multicomponent polynomial-phase signal modeling," *IEEE Trans. Signal Process.*, vol. 46, no. 3, pp. 691–708, Mar. 1998.

[3] B. Boashash and P. O'Shea, "Polynomial Wigner-Ville distributions and their relationship to time-varying higher order spectra," *IEEE Trans. Signal Process.*, vol. 42, no. 1, pp. 216–220, Jan. 1994.

[4] M. Benidir and A. Ouldali, "Polynomial phase signal analysis based on the polynomial derivatives decompositions," *IEEE Trans. Signal Process.*, vol. 47, no. 7, pp. 1954–1965, Jul. 1999.

[5] B. Barkat and B. Boashash, "Design of higher order polynomial Wigner-Ville distributions," *IEEE Trans. Signal Process.*, vol. 47, no. 9, pp. 2608–2611, Sep. 1999.

[6] P. O'Shea, "A new technique for instantaneous frequency rate estimation," *IEEE Signal Process. Lett.*, vol. 9, no. 8, pp. 251–252, Aug. 2002.

[7] ——, "A fast algorithm for estimating the parameters of a quadratic FM signal," *IEEE Trans. Signal Process.*, vol. 52, no. 2, pp. 385–393, Feb. 2004.

[8] J. Angeby, "Estimating signal parameters using the nonlinear instantaneous least squares approach," *IEEE Trans. Signal Process.*, vol. 48, no. 10, pp. 2721–2732, Oct. 2000.

[9] T. Abatzoglou, "Fast maximum likelihood joint estimation of frequency and frequency rate," in *Proc. IEEE Int. Conf. ICASSP*, 1986.

[10] S. Peleg and B. Porat, "Linear FM signal parameter estimation from discrete-time observations," *IEEE Trans. Aerosp. Electron. Syst.*, vol. 27, no. 4, pp. 607–616, Jul. 1991.

Estimating Statistical Properties of Eddy-Current Signals From Steam Generator Tubes

Aleksandar Dògandžić and Ping Xiang

***Abstract*—We develop a model for characterizing amplitude and phase probability distributions of eddy-current signals and propose a maximum likelihood (ML) method for estimating the amplitude and phase distribution parameters from measurements corrupted by additive complex white Gaussian noise. The squared amplitudes and phases of the potential defect signals are modeled as independent, identically distributed (i.i.d.) random variables following gamma and von Mises distributions, respectively. Newton–Raphson iteration is utilized to compute the ML estimates of the unknown parameters. We also compute Cramér–Rao bounds (CRBs) for the unknown parameters and discuss initialization of the Newton–Raphson iteration. The proposed method is applied to analyze rotating-probe eddy-current data from steam-generator tube inspection in nuclear power plants. The obtained estimates can be utilized for maximum *a posteriori* (MAP) signal phase and amplitude estimation, as well as efficient feature extractors in a defect classification scheme. We present numerical examples with both real and simulated data to demonstrate the performance of the proposed methods.**

***Index Terms*—Eddy-current signal modeling, maximum likelihood parameter estimation, Newton–Raphson iteration.**

I. INTRODUCTION

In eddy-current based nondestructive evaluation of materials, a flaw is usually detected by observing probe impedance changes caused by the interaction between induced oscillating electric current in a conductor and a defect [1], [2]. Eddy-current inspection is performed extensively to detect and size flaws in steam-generator tubes in nuclear power plants [3], [4]. Rotating-probe eddy-current testing has been proposed to improve the detection, interpretation, and sizing of defects [3]. (For related analytical and numerical solutions to the eddy-current testing problem, see, e.g., [1], [5]–[8], and references therein.) Rotating probes usually consist of three coils spaced $2\pi/3$ rad (120°) apart, as shown in Fig. 1. Each coil scans the inner surface of the tube by moving along a helical path. To extract meaningful information from the rotating-probe data, a preprocessing step is performed first [4]. The raw data is one-dimensional (1-D) in nature, and a synchronization step converts it to a two-dimensional (2-D) image, where each column of the resulting image contains the data from one rotation. Fig. 2 illustrates the result of this process. Fig. 2(a) and (b) show the raw 1-D signal and synchronized 2-D image, respectively. Fig. 2(c) is a result of calibration where potential defect signals show up; the details of the calibration process are described in [4]. In Fig. 3, we present impedance-plane plots of typical signals measured by the rotating-probe eddy-current system. Further analysis of the potential defect signals is needed to discriminate between defects and nondefects, as well as between different kinds of defects. In this correspondence (see also [9]), we propose a statistical model for characterizing amplitude and phase probability distributions of eddy-current signals. We model the squared amplitudes and

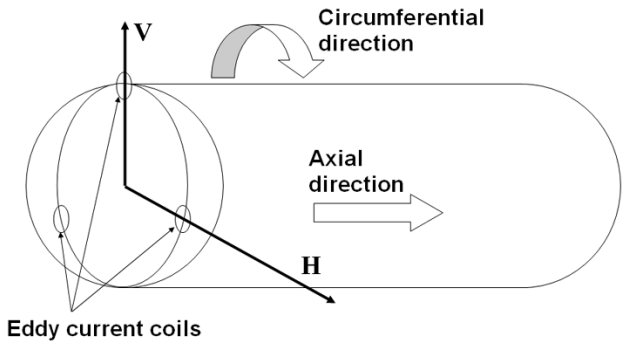

Fig. 1. Rotating-probe eddy-current system.

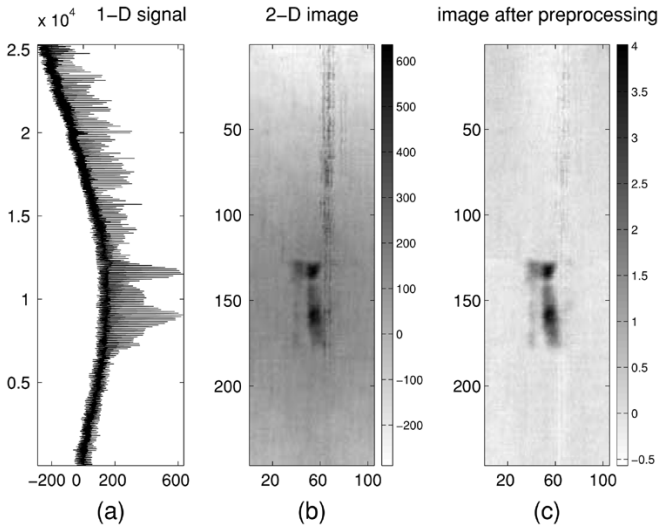

Fig. 2. Signal preprocessing. (a) 1-D raw data. (b) 2-D image. (c) 2-D image after preprocessing.

Manuscript received June 8, 2004; revised November 2, 2004. This work was supported by the NSF Industry-University Cooperative Research Program, Center for Nondestructive Evaluation, Iowa State University. The associate editor coordinating the review of this manuscript and approving it for publication was Prof. Tulay Adali.

The authors are with the ECpE, Department of Electrical and Computer Engineering, Iowa State University, Ames, IA 50011 USA (e-mail: ald@iastate.edu; pxiang@iastate.edu).

Digital Object Identifier 10.1109/TSP.2005.851173